applied sciences

MDPI

Article

Reconstruction of the Physiological Behavior of Real and Synthetic Vessels in Controlled Conditions

Andrzej Polanczyk [1,*,†], Aleksandra Piechota-Polanczyk [2,†], Agnieszka W. Piastowska-Ciesielska [2], Ihor Huk [3], Christoph Neumayer [3], Julia Balcer [4] and Michal Strzelecki [4]

1 The Faculty of Safety Engineering and Civil Protection, Fire University, 01-629 Warsaw, Poland
2 Department of Cell Cultures and Genomic Analysis, Medical University of Lodz, 90-752 Lodz, Poland; aleksandra.piechota-polanczyk@umed.lodz.pl (A.P.-P.); agnieszka.piastowska@umed.lodz.pl (A.W.P.-C.)
3 Department of Surgery, Division of Vascular Surgery, Medical University of Vienna, Spitalgasse 23, 1090 Vienna, Austria; ihor.huk@agamemnon.at (I.H.); christoph.neumayer@meduniwien.ac.at (C.N.)
4 Institute of Electronics, Lodz University of Technology, 93-590 Lodz, Poland; julia_balcer@wp.pl (J.B.); michal.strzelecki@p.lodz.pl (M.S.)
* Correspondence: andrzej.polanczyk@gmail.com
† These authors contributed equally to this work.

Abstract: The objective of this study is to assess the ability of an Artificial Circulatory Phantom (ACP) to verify its accuracy in simulating the movement of artificial vessels vs. real vessels under changing cardiovascular parameters such as heartbeat, ejection fraction, and total peripheral resistance. The experiments were conducted with blood-like fluid that flows through two types of vessels: iliac arteries and different types of ePTFE vascular prostheses. Parameters such as diameter and tortuosity were measured and analyzed. The flow characteristics included a pulsating pattern with a frequency of 60–120 min^{-1} and ejection volumes ranging from 70 to 115 mL. The results showed a predominantly positive correlation between wall displacement (W_d) and tortuosity index (T_i) for the iliac artery (R^2 = 0.981), as well as between Wd and mean tortuosity index (MT_i) (R^2 = 0.994). Similarly, positive correlations between Wd and T_i (R^2 = 0.942) and Wd and MT_i (R^2 = 0.922) were computed for the ePTFE vascular prosthesis. The ACP introduced in this study is a valuable tool for evaluating various vessel types and the spatial configurations of vascular prostheses under diverse hemodynamic conditions. These findings are promising for the advancement of novel approaches to the testing and design of vascular grafts, ultimately enhancing their patency rates in future applications.

Keywords: vascular imaging; vascular prosthesis; PTFE vascular prosthesis; tortuosity; stress measurement; stress control; wall displacement; artificial vascular system

Citation: Polanczyk, A.; Piechota-Polanczyk, A.; Piastowska-Ciesielska, A.W.; Huk, I.; Neumayer, C.; Balcer, J.; Strzelecki, M. Reconstruction of the Physiological Behavior of Real and Synthetic Vessels in Controlled Conditions. *Appl. Sci.* **2024**, *14*, 2600. https://doi.org/10.3390/app14062600

Academic Editor: Gang Wei

Received: 17 February 2024
Revised: 15 March 2024
Accepted: 16 March 2024
Published: 20 March 2024

1. Introduction

Human organs are complex structures composed of specialized cells that collaboratively execute unique functions that are crucial for survival [1]. Ethical considerations necessitate the utilization of bio-tissue and mechanical systems that can replicate the physiological and pathophysiological aspects of organs [2]. Such systems hold the potential to provide enhanced predictive capabilities for human tissue responses compared to existing testing methodologies. Substantial progress has been made in microfluidic technologies, particularly in the context of organ-on-a-chip devices [3]. Each vascular product requires an individualized bioreactor [4]. Many important considerations should be included in the bioreactor's construction [5]. Bioreactors for vascular products, as well as vascular grafts, commonly represent a pulsatile system [6]. Different parameters that are important for patients may be monitored in vitro, e.g., perfusion for different hemodynamic conditions, as well as the graft's mechanical properties [7]. Such an approach minimizes the risk of failure during surgery.

In the realm of medical diagnostics, the integration of various techniques, such as ultrasonography [8], 3D ultrasound [9], 4D ultrasound strain (4D-US) [10], and echocardiography, is gaining popularity [11]. Combining these methods with engineering approaches, such as computational fluid dynamics (CFD), has the potential to enhance analyses and contribute to patient diagnosis [12–14]. These approaches are commonly employed for predicting therapeutic outcomes in cases of aortic-wall-associated injuries, such as aneurysms or wall ruptures [15]. However, limited efforts have been directed toward leveraging ex vivo systems to faithfully replicate blood flow parameters and investigate flow and pressure conditions in an artificial environment [16]. Moreover, most investigated models primarily reconstruct laminar flow or focus on graft preservation solutions [17,18]. Conversely, the pulsatile nature of blood hemodynamics in the cardiac system indicates the significant stretching of vessel walls, potentially leading to wall damage, especially in the presence of pre-existing conditions like atherosclerosis [19]. Furthermore, existing systems in the literature often only reconstruct laminar flow through artificial vessels or grafts [20], meaning that the relationship between elastic storage and the viscous dissipation of energy transmitted to vessel walls during systole in the cardiac cycle is not fully understood [21].

This study aims to verify its accuracy in simulating the movement of artificial vessels vs. real vessels under changing cardiovascular parameters such as heartbeat, ejection fraction, and total peripheral resistance. The experiments were conducted with blood-like fluid that flows through two types of vessels: iliac arteries and different types of ePTFE vascular prostheses.

The remainder of the manuscript is organized as follows: Section 2, Materials and Methods, outlines the experimental setup, the initial and boundary conditions, and the description of statistical analyses. Section 3, Results, presents the obtained results; Section 4, Discussion, contextualizes the findings within the current state-of-the-art; and Section 5, Conclusions, summarizes the paper.

2. Materials and Methods

2.1. Experimental Set-Up

An Artificial Circulatory Phantom (ACP) (Figure 1), designed to simulate the functioning of a segment of the human cardiovascular system, was constructed explicitly for this project and comprehensively detailed in our previous work [22]. In essence, at the core of the setup, a transparent rectangular vessel reactor, constructed from Plexiglas and equipped to maintain a constant temperature (temperature was measured with an installed temperature sensors), was positioned. The reactor was filled with a non-commercial fluid designed to mimic the rheological properties of blood. This fluid comprised 60% distilled water and 40% glycerol, presenting a density of 1.2 g cm^{-3} and a viscosity of 4.8×10^{-3} Pa·s. The fluid was supplied from a fluid chamber via a pump. The pulsating character of the flow was achieved by self-made artificial heart. This device manifested as a moving plunger housed in a stainless-steel corpus and driven by an electric motor, controlled discharge pressure, discharge volume, and the pulsation of prediction. These parameters were controlled by an electrical engine connected to the computer. Each time, a specified amount of the medium supplies the analyzed vessels, as well as ePTFE vascular prosthesis.

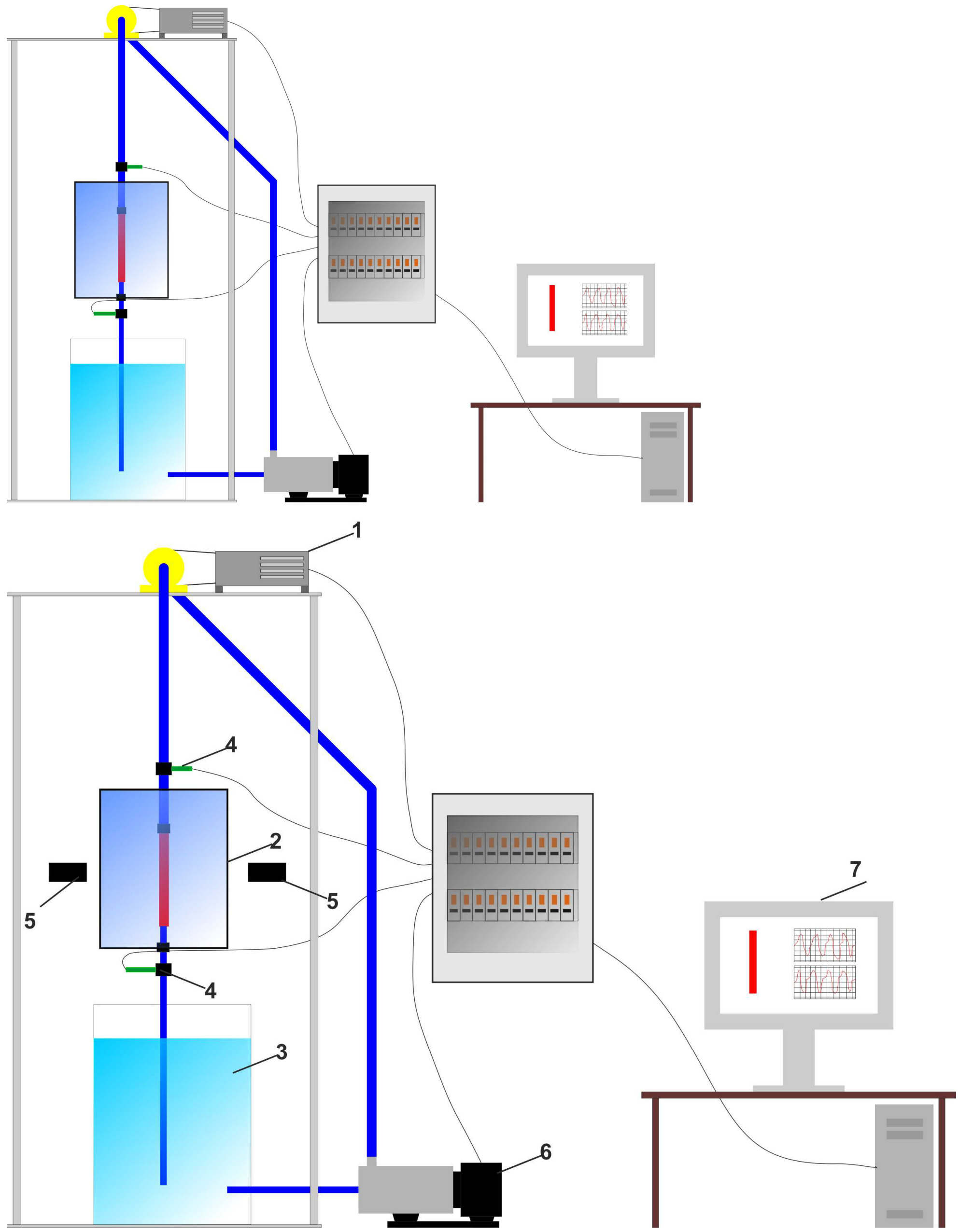

Figure 1. An artificial circulatory phantom (ACP). The system comprised the following: 1—an artificial heart; 2—a transparent, rectangular chamber for the vessel; 3—a transparent container with distilled water and glycerol; 4—temperature sensors; 5—a camera; 6—a pump for distilled water and glycerol; 7—computer.

The vision system (VS) incorporated nine cameras positioned on an aluminum circular profile parallel to the floor, enabling horizontal movement [19]. The size of a pixel in the captured images of the real object was 0.35 mm. To increase the accuracy of vision acquisition, cameras were able to move 10 deg. Steps were included to both sides in the range of 40 deg. The entire system was controlled by a portable workstation (Dell Precision M6400 (Dell, Round Rock, TX, USA)) equipped with a four-core Intel CPU (2.4 GHz), 4 GB RAM (1333 MHz), and a 500 GB SSD HD. A self-developed acquisition and control software (ACS) facilitated the operation of the system.

2.2. Material

Two types of materials were investigated: iliac arteries (Figure 2a) and expanded polytetrafluoroethylene arterial (ePTFE) vascular prostheses (Figure 2b). Iliac arteries, with a diameter of 8 mm, thickness of 1 mm, and length of 100 mm, were procured from six male organ donors (mean age 50 ± 10 years) at the Medical University of Vienna. These arteries were promptly mounted in the experimental set-up, and all experiments were conducted within 24 h of their harvest from the six donor organs.

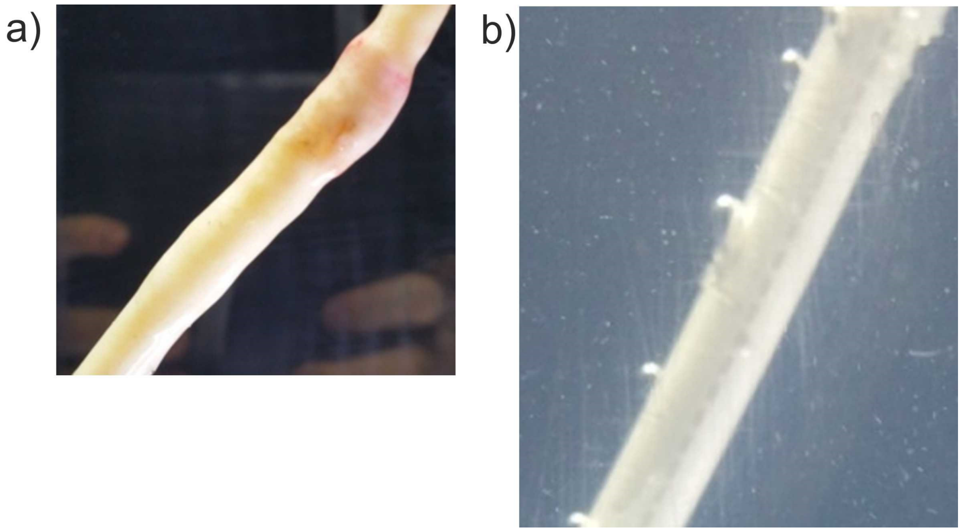

Figure 2. An artificial circulatory phantom (ACP): (**a**) iliac artery; (**b**) expanded polytetrafluoroethylene arterial (ePTFE) vascular prosthesis.

For comparison, six ePTFE vascular prostheses, commonly employed materials in vascular surgeries, were utilized. These prostheses had a diameter of 8 mm, thickness of 0.1 mm, and length of 100 mm. In total, six iliac arteries and six ePTFE vascular prostheses underwent investigation in this study.

2.3. Experimental Conditions

Changes in the diameter and displacement of the walls of the iliac arteries were investigated and compared with vascular prostheses made of expanded polytetrafluoroethylene (ePTFE) with a specified length of 100 mm, diameter of 8 mm, and wall thickness of 1 mm. The analysis encompassed iliac arteries sharing identical dimensions (length of 100 mm and diameter of 8 mm). The study received approval from the local Institutional Review Board (2069/2012) of the Medical University of Vienna. To validate the accuracy of the experimental setup, vision data were juxtaposed with clinical data obtained using the ultrasound 2D- Speckle tracking technique (2DSTT) (GE Vivid 7, GE Healthcare, Pittsburgh, PA, USA), equipped with software for strain analysis (EchoPac PC, GE Medical System, Pittsburgh, PA, USA, https://www.gehealthcare.com/products/ultrasound/vivid/echopac, accessed on 16 February 2024).

To verify the area change percentage (ACP) and vessel shape (VS), flow construction was performed with various parameters: pulsatile nature heart rates (FP)—60, 75, 90, 105, and 120 min^{-1}—and different stroke volumes (volumes (EV): 70, 85, 100 and 115 mL) using non-commercial fluid for one cycle. The movement of the vessel wall was analyzed using 2DSTT, and it was ascertained whether the changes recorded with VS replicated the wall changes recorded with 2DSTT. Furthermore, current studies indicate that pulsatile flow plays a crucial role in the evaluation of pathological states, e.g., aneurysms [23].

For standardization, the changes in vessel diameter recorded by the ACP were compared with clinical data collected during patient examinations using the 2DSTT approach.

Six ACP iliac arteries were compared with data from six healthy patients diagnosed with 2DSTT using the same type of arteries and hemodynamic conditions as in the ACP.

To further standardize the results for ACP patients and healthy subjects, tests were conducted under the conditions of heart rates (75 min^{-1} and 90 min^{-1}) and stroke volume (EV = 70 mL). Medical data were then compared with the ACP results obtained under the same hemodynamic conditions. Ultimately, 120 cases were studied for iliac arteries and 120 cases for the ePTFE vascular prostheses.

The diameter change (Dc) (Equation (1)) and wall displacement (Wd) (Equation (2)) were calculated using the following equations:

$$\mathrm{Dc} = \mathrm{Ddynamic(x,y,z)} - \mathrm{Dstatic(x,y,z)} \tag{1}$$

where:

Dc—vessel's diameter change [mm].
Dstatic(x,y,z)—vessel's diameter, recorded under static conditions [mm].
Ddynamic(x,y,z)—the maximal vessel's diameter under dynamic conditions [mm].

$$\mathrm{Wd} = \mathrm{Wdynamic}\ (\mathrm{xp}',\mathrm{yp}',\mathrm{zp}') - \mathrm{Wstatic}\ (\mathrm{xp},\mathrm{yp},\mathrm{zp}) \tag{2}$$

where:

Wd—vessel's wall displacement [mm].
Wstatic (xp,yp,zp)—spatial configuration of vessel's wall in relation to its central axis, recorded under static conditions [mm].
Wdynamic (xp′,yp′,zp′)—spatial configuration of vessel's wall in relation to its central axis, recorded under dynamic conditions [mm].

Moreover, tortuosity (Tortuosity index T_i (Equation (3)); Tortuosity (T) (Equation (4)) was applied to verify the correct operation of the WD parameter measurement.

$$T_i = L/C \tag{3}$$

where:

T_i—tortuosity index [-].
L—the linear distance of the vessel's segment [mm].
C—the distance between vessel's start and endpoint [mm].

$$T = 1 - d/l \tag{4}$$

where:

T—tortuosity [-].
d—the linear distance of the centerline [-].
L—the distance along the centerline [-].

Furthermore, a modification of the tortuosity (modified tortuosity index (Mti) (Equation (5))) presented in the literature was proposed.

$$MT_i = L/C + 1/R \tag{5}$$

where:

MT_i—modified tortuosity index [mm^{-1}].
L, C—as defined in Equation (3).
R—the reciprocal of the radius of curvature at a particular point on the centerline of the analyzed vessel.

2.4. Statistical Analysis

Statistica 12.0 software (Tulsa, OK, USA) was used for statistical calculations. The results are presented as mean ± SD. The Bland–Altman method was used to assess the compatibility between the experimental setup and the 2DSTT technique. Additionally, a simple linear regression analysis was conducted to examine the correlation. Comparisons between the analyzed groups were performed using the Kolmogorov–Smirnov test after confirming normality and variance. Statistical significance was considered when $p < 0.05$, unless stated otherwise.

3. Results

3.1. Diameter Dilatation

The mean measured D_c (for FP = 75 min^{-1}) for the iliac arteries was 0.94 ± 0.02 mm when calculated with the set-up and 0.92 ± 0.01 mm when calculated with 2DSTT (p = 0.069). The mean D_c (for FP = 75 min^{-1}) for the ePTFE vascular prosthesis was 0.44 ± 0.01 mm when calculated with the set-up and 0.43 ± 0.01 mm when calculated with 2DSTT (p = 0.022). Moreover, the mean measured D_c (for FP = 90 min^{-1}) for the iliac arteries was 1.04 ± 0.01 mm when calculated with the set-up and 1.02 ± 0.02 mm when calculated with 2DSTT (p = 0.022). The mean D_c (for FP = 90 min^{-1}) for the ePTFE vascular prosthesis was 0.49 ± 0.01 mm when calculated with the set-up and 0.48 ± 0.01 mm when calculated with 2DSTT (p = 0.999) (Table 1).

Table 1. Diameter dilatation for the iliac artery and ePTFE vascular prosthesis. Values are measured in millimeters.

Frequency of Pulsation [1/s]	Ejection Volume [mL]	Diameter of Iliac Artery (Measured with Set-Up) [mm]	Diameter of Iliac Artery (Measured with 2DSTT) [mm]	Diameter of ePTFE Vascular Prosthesis (Measured with Set-Up) [mm]	Diameter of ePTFE Vascular Prosthesis (Measured with 2DSTT) [mm]
75	70	0.89	0.91	0.42	0.56
75	70	0.92	0.93	0.41	0.53
75	70	0.93	0.95	0.43	0.51
75	70	0.93	0.95	0.42	0.52
75	70	0.92	0.95	0.44	0.54
75	70	0.92	0.94	0.43	0.51
90	70	0.99	1.04	0.48	0.48
90	70	1.02	1.03	0.48	0.49
90	70	1.01	1.03	0.49	0.48
90	70	1.01	1.03	0.49	0.48
90	70	1.04	1.04	0.48	0.49
90	70	1.03	1.06	0.48	0.49

The Bland–Altman analysis for FP = 75 min^{-1} and FP = 90 min^{-1} indicated that the records gathered with the set-up and 2DSTT for the iliac arteries were comparable. The difference between the set-up and 2DSTT was equal to 0.02 mm for the range equal to 0.04 mm (Figure 3a), while for FP = 90 min^{-1}, it was 0.04 mm for the range equal to 0.13 mm (Figure 3b). Moreover, the difference between the set-up and 2DSTT for ePTFE vascular prostheses was equal to 0.01 mm for the range equal to 0.03 mm (Figure 3c), while for FP = 90 min^{-1}, it was 0.01 mm for the range equal to 0.04 mm (Figure 3d).

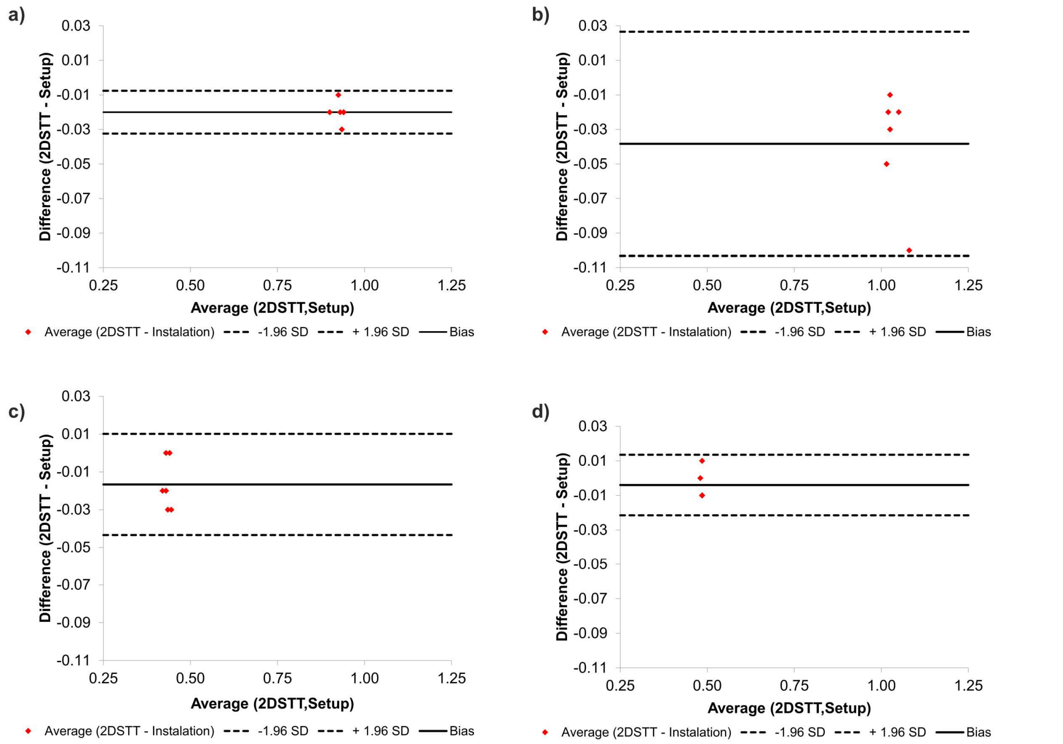

Figure 3. Comparison of set-up and 2DSTT for: (**a**) iliac arteries for FP = 75 min^{-1}; (**b**) iliac arteries for FP = 90 min^{-1}; (**c**) ePTFE vascular prosthesis for FP = 75 min^{-1}; (**d**) ePTFE vascular prosthesis for FP = 90 min^{-1} with the use of Bland–Altman analysis. The analyzed group consisted of n = 6. Statistical significance was considered for all analyses with a threshold of $p < 0.05$.

3.2. Wall Displacement

Firstly, wall displacement was measured with the Set up (Table 2). For iliac arteries with different frequencies of pulsation, a similar wall displacement was observed (for 60 s^{-1}, 75 s^{-1}, 90 s^{-1}, 105 s^{-1}, and 120 s^{-1}, 0.142 ± 0.002 mm, 0.144 ± 0.003 mm, 0.144 ± 0.004 mm, 0.142 ± 0.002 mm, and 0.141 ± 0.004 mm, respectively) (Figure 4a,b). For ePTFE vascular prostheses, an increase in the frequency of pulsation led to a decrease in wall displacement (for 60 s^{-1}, 75 s^{-1}, 90 s^{-1}, 105 s^{-1} and 120 s^{-1}, 0.741 ± 0.190 mm, 0.683 ± 0.107 mm, 0.670 ± 0.095 mm, 0.593 ± 0.103 mm and 0.600 ± 0.071 mm, respectively) (Figure 4c,d).

Table 2. Wall displacement for the iliac artery and ePTFE vascular prosthesis. Values are measured in millimeters.

Frequency of Pulsation [1/s]	Ejection Volume [mL]	Wall Displacement for Iliac Artery (Measured with Set-Up) [mm]	Wall Displacement for ePTFE Vascular Prosthesis (Measured with Set-Up) [mm]
75	70	0.14	0.56
75	70	0.15	0.53
75	70	0.15	0.51
75	70	0.15	0.52
75	70	0.15	0.54
75	70	0.15	0.51
90	70	0.14	0.39
90	70	0.14	0.38
90	70	0.14	0.40
90	70	0.14	0.40
90	70	0.14	0.39
90	70	0.14	0.40

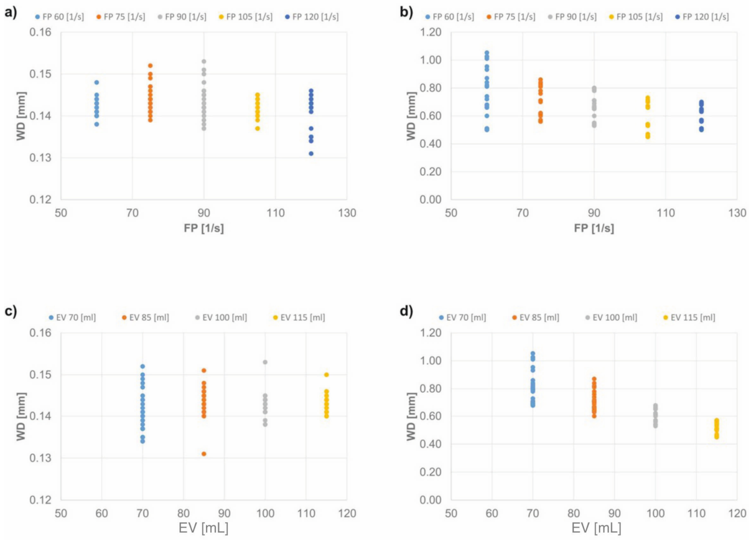

Figure 4. The wall displacement (WD) of: (**a**) iliac arteries as function of frequency of pulsation (FP) for FP = 75 min^{-1}; (**b**) iliac arteries as a function of frequency of pulsation (FP) for FP = 90 min^{-1}; (**c**) ePTFE vascular prosthesis as a function of frequency of pulsation (FP) for FP = 75 min^{-1}; (**d**) ePTFE vascular prosthesis as a function of frequency of pulsation (FP) for FP = 90 min^{-1}; analyzed cases consisted of n = 120.

An example of the analyzed objects (iliac artery and ePTFE vascular prosthesis) is presented in Figures 5 and 6. The degree of deformation was illustrated with triangles. Each time, greater flexibility of the iliac arteries was observed compared to the ePTFE vascular prostheses.

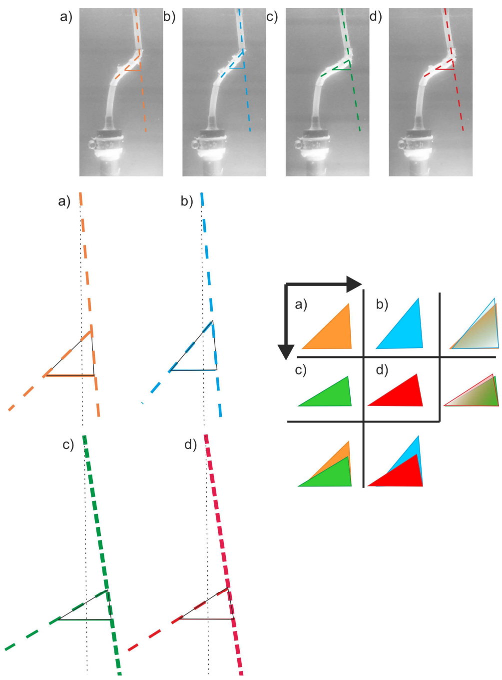

Figure 5. An example of the iliac artery movement for: (**a**) EV = 70 mL, FP = 60 min^{-1}; (**b**) EV = 70 mL, FP = 75 min^{-1}; (**c**) EV = 85 mL, FP = 60 min^{-1}; (**d**) EV = 85 mL, FP = 75 min^{-1}. For each analyzed case, two centerlines were added. Centerlines illustrate how the vessel works for different hemodynamic parameters. Moreover, triangles were added to illustrate the degree of the vessel's deformation/bent as area under the centerlines. Colors for each case were as follows: orange—EV = 70 mL, FP = 60 min^{-1}; blue—EV = 70 mL, FP = 75 min^{-1}; green—EV = 85 mL, FP = 60 min^{-1}; red—EV = 85 mL, FP = 75 min^{-1}.

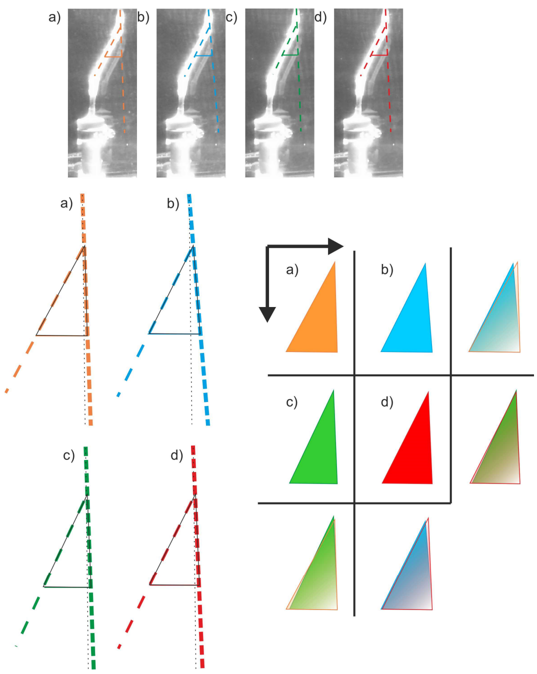

Figure 6. An example of ePTFE vascular prosthesis movement for: (**a**) EV = 70 mL, FP = 60 min^{-1}; (**b**) EV = 70 mL, FP = 75 min^{-1}; (**c**) EV = 85 mL, FP = 60 min^{-1}; (**d**) EV = 85 mL, FP = 75 min^{-1}. For each analyzed case, two centerlines were added. The centerlines illustrate how ePTFE vascular prosthesis works for different hemodynamic parameters. Moreover, triangles were added to illustrate the degree of ePTFE vascular prosthesis's deformation/bent as the area under the centerlines. Colors for each case are as follows: orange—EV = 70 mL, FP = 60 min^{-1}; blue—EV = 70 mL, FP = 75 min^{-1}; green—EV = 85 mL, FP = 60 min^{-1}; red—EV = 85 mL, FP = 75 min^{-1}.

3.3. Tortuosity

Initially, the analysis focused on the tortuosity and tortuosity index. Notably, the average tortuosity and tortuosity index for the iliac arteries were comparable, reaching the level of 0.86 $\pm$ 0.02. Conversely, for ePTFE vascular prostheses, both the average tortuosity and tortuosity index were almost 3.5 times lower (0.24 $\pm$ 0.06) compared to the iliac arteries (p = 0.0001). Subsequently, the modified tortuosity index was examined, revealing that, for iliac arteries, the average modified tortuosity index was 0.87 $\pm$ 0.02. In contrast, for ePTFE vascular prostheses, the average modified tortuosity index and tortuosity indexes were 0.28 $\pm$ 0.05 (p = 0.0001).

The Bland–Altman analysis demonstrated minimal significant differences between Ti and MTi for iliac arteries. The discrepancy between Ti and MTi was 0.01, within the range of 0.02 (Figure 7a). In contrast, for ePTFE vascular prostheses, the difference between Ti and Mti was 0.04, within the range of 0.09 (Figure 7b).

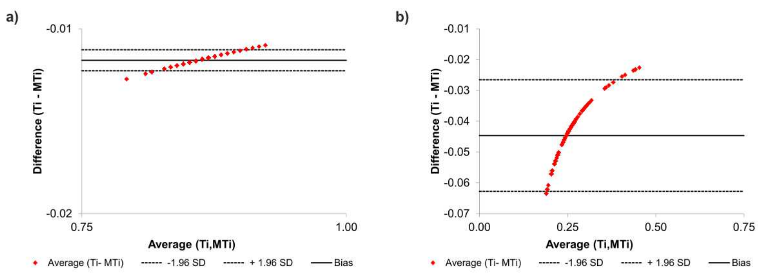

Figure 7. Comparison of tortuosity index (T_i) and modified tortuosity index (MT_i) for: (**a**) iliac arteries with the use of Bland–Altman analysis; (**b**) ePTFE vascular prosthesis with the use of Bland–Altman analysis. The analyzed cases consisted of n = 120. Statistical significance was considered for all analyses with a threshold of p < 0.05.

Moreover, W_d was compared to T, T_i as well as MT_i. Since the results of T and T_i were the same, T_i was used for further calculations. For the iliac artery, a positive correlation between W_d and T_i was calculated (R^2 = 0.981). Similarly, for ePTFE vascular prostheses, a positive correlation between W_d and MTi (R^2 = 0.994) (Figure 8a), W_d and T_i (R^2 = 0.942), and W_d and MT_i was observed (R^2 = 0.922) (Figure 8b).

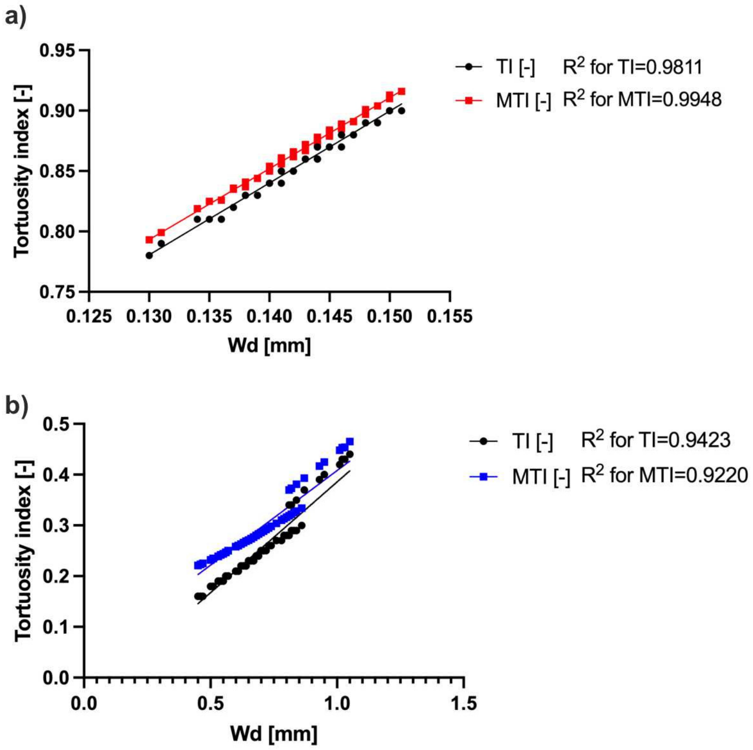

Figure 8. Correlation for: (**a**) the iliac arteries for the tortuosity index as function of wall deformation; (**b**) for the ePTFE vascular prosthesis for the tortuosity index as function of wall deformation. Scatterplot graphic; analyzed cases consisted of n = 120.

4. Discussion

In our earlier investigations, we demonstrated the ability of an ex vivo bioreactor to recreate hemodynamics in elastic 3D-printed models of abdominal aortic aneurysms [24,25] and human grafts [22]. In those papers, we showed that our self-made system allows us to successfully track hemodynamic changes in the abdominal aortic aneurysm (AAA) model with thrombus or stent-graft under different hemodynamic conditions. Here, we aimed to verify the accuracy of our platform to simulate the movement of artificial vessels in relation to a real vessel under changing cardiovascular parameters such as heartbeat, ejection fraction, and total peripheral resistance.

The integration of engineering and medical tools could offer a valuable method for the ex vivo analysis of biomaterials. [26]. Nevertheless, artificial systems have limitations, such as the specificity of their construction, the absence of a pulsating flow [27], or their reliance on animal tissues rather than human tissues [28]. Additionally, while MRI techniques offer data regarding the spatial configuration of vessels, they do not provide information about their stability or rupture [29]. The present research confirms that the Artificial Circulatory Phantom effectively replicates blood hemodynamics, allowing for the recreation of physiological conditions, such as the ejection volume, pulsation frequency, and ejection pressure for iliac arteries and ePTFE vascular prostheses. This corresponds with findings from comparable studies conducted by other researchers [11,30,31].

Significantly, we noted that the achievement of physiological conditions required the utilization of a water environment, an innovative approach with no prior literature precedent for simulating organ tension. For instance, Piola et al. devised a culture system to replicate hemodynamic conditions in saphenous veins following coronary artery bypass grafting [16,32]. Mundagi et al. investigated cellular interactions in pig carotid arteries using an ex vivo system, with flow reconstructed using a peristaltic pump at a constant speed [33]. However, these studies lacked an authentic representation of the heartbeat, which is a distinctive feature of our approach. Similarly, Bihari et al. examined abdominal aortic aneurysm displacement using 3D speckle-tracking ultrasound [31], but their horizontal vessel configuration differed from our vertical positioning.

Moreover, Genovese et al. applied a dedicated system for mouse artery stress analysis [34]. Gulan et al. studied the transparent part of the cardiac system using 3D particle-tracking velocimetry [35], but their methodology lacked a water environment and the measurement of vessel spatial configuration.

Taking into account the significance of the vessel's physical properties for the reconstruction of clinical conditions [36,37], our study is consistent with the observations made by Pahlevan et al. [37], who identified changes in the aortic pressure wave associated with varying aortic stiffness, and Li et al. [38], who documented the age-related stiffening of the ascending aorta. Kashyap et al. [39] analyzed the accuracy of the tortuosity index in the left main coronary artery using computational modeling, contrasting with our results, which indicated a good agreement between the experimental and clinical data. Additionally, our study differs from the findings of Malve et al. and Pinho et al. [40,41], who noted higher averages and wider spreads of the WSS values.

In light of our presented results, we suggest that it is essential to examine other geometric parameters, such as angulations, in our system to accurately predict the occurrence of thrombus or prosthesis movement.

Limitation of the Study

The examined arteries and ePTFE vascular prostheses were limited to a length of 100 mm due to the dimensions of the chamber. This constraint was dictated by the design of the Artificial Circulatory Phantom (ACP). To increase the flexibility of the ACP, modifications should be considered for vessels of both shorter and longer lengths in future iterations. Furthermore, the inlet and outlet pipes were designed for vessels within the size range of the iliac arteries, limiting their suitability for smaller vessels. To expand the applicability of the ACP, additional adjustments to accommodate smaller vessels are necessary.

5. Conclusions

The Artificial Circulatory Phantom (ACP) presented in this article demonstrates the potential to be a valuable tool for evaluating different types of vascular prostheses under defined boundary and initial conditions. The ability to independently vary the frequency of pulsation and the ejection volume within the ACP unveiled distinct mechanical responses in iliac artery grafts and vascular prostheses. These insights offer valuable information that can contribute to the exploration of novel approaches in the design of vascular grafts, ultimately aiming to improve their patency rates in future applications. In the future, we plan to use our self-made equipment to test selected types of vascular prostheses.

Author Contributions: Conceptualization, A.P., A.W.P.-C. and A.P.-P.; methodology, I.H. and C.N.; software, M.S.; validation, A.P., A.P.-P. and M.S.; formal analysis, A.P.; investigation, A.P.; resources, A.P.; data curation, I.H. and C.N.; writing—original draft preparation, A.P., A.P.-P., I.H., C.N. and M.S.; writing—review and editing, A.P., A.P.-P., I.H., C.N., A.W.P.-C. and M.S.; visualization, A.P., A.P.-P. and J.B.; supervision, M.S.; project administration, A.P. and M.S.; funding acquisition, M.S. All authors have read and agreed to the published version of the manuscript.

Funding: The study was supported by the Polish National Centre for Research and Development (501/10-34-19-605 to AP) and by grant number 181110 from the Medical University of Vienna, Department of Surgery, Division of Vascular Surgery (to IH).

Institutional Review Board Statement: The study was approved by the local Institutional Review Board (2069/2012) of the Medical University of Vienna.

Informed Consent Statement: Informed consent was obtained from all subjects involved in the study.

Data Availability Statement: The data used to support the findings of this study are available from the corresponding author upon request.

Conflicts of Interest: The authors declare no conflicts of interest.

References

1. Astashkina, A.; Mann, B.; Grainger, D.W. A Critical Evaluation of In Vitro Cell Culture Models for High-Throughput Drug Screening and Toxicity. *Pharmacol. Ther.* **2012**, *134*, 82–106. [CrossRef]
2. Jung, S.-M.; Chung, G.Y.; Shin, H.S. Artificial Controlled Model of Blood Circulation System for Adhesive Evaluation. *Sci. Rep.* **2017**, *7*, 16720. [CrossRef] [PubMed]
3. Sakolish, C.M.; Esch, M.B.; Hickman, J.J.; Shuler, M.L.; Mahler, G.J. Modeling Barrier Tissues In Vitro: Methods, Achievements, and Challenges. *EBioMedicine* **2016**, *5*, 30–39. [CrossRef]
4. Ratcliffe, A.; Niklason, L.E. Bioreactors and Bioprocessing for Tissue Engineering. *Ann. N. Y. Acad. Sci.* **2002**, *961*, 210–215. [CrossRef]
5. Fish, J.; Halberstadt, C.; McCoy, D.W.; Robbins, N. Bioreactor Design Considerations for Hollow Organs. *Methods Mol. Biol.* **2013**, *1001*, 207–214. [CrossRef]
6. Diamantouros, S.E.; Hurtado-Aguilar, L.G.; Schmitz-Rode, T.; Mela, P.; Jockenhoevel, S. Pulsatile Perfusion Bioreactor System for Durability Testing and Compliance Estimation of Tissue Engineered Vascular Grafts. *Ann. Biomed. Eng.* **2013**, *41*, 1979–1989. [CrossRef]
7. Maschhoff, P.; Heene, S.; Lavrentieva, A.; Hentrop, T.; Leibold, C.; Wahalla, M.; Stanislawski, N.; Blume, H.; Scheper, T.; Blume, C. An Intelligent Bioreactor System for the Cultivation of a Bioartificial Vascular Graft. *Eng. Life Sci.* **2016**, *17*, 567–578. [CrossRef]
8. Karatolios, K.; Wittek, A.; Nwe, T.H.; Bihari, P.; Shelke, A.; Josef, D.; Schmitz-Rixen, T.; Geks, J.; Maisch, B.; Blase, C.; et al. Method for Aortic Wall Strain Measurement with Three-Dimensional Ultrasound Speckle Tracking and Fitted Finite Element Analysis. *Ann. Thorac. Surg.* **2013**, *96*, 1664–1671. [CrossRef]
9. Rouet, L.; Mory, B.; Attia, E.; Bredahl, K.; Long, A.; Ardon, R. A Minimally Interactive and Reproducible Method for Abdominal Aortic Aneurysm Quantification in 3D Ultrasound and Computed Tomography with Implicit Template Deformations. *Comput. Med. Imaging Graph.* **2017**, *58*, 75–85. [CrossRef]
10. Derwich, W.; Wittek, A.; Pfister, K.; Nelson, K.; Bereiter-Hahn, J.; Fritzen, C.P.; Blase, C.; Schmitz-Rixen, T. High Resolution Strain Analysis Comparing Aorta and Abdominal Aortic Aneurysm with Real Time Three Dimensional Speckle Tracking Ultrasound. *Eur. J. Vasc. Endovasc. Surg.* **2016**, *51*, 187–193. [CrossRef]
11. Fadel, B.M.; Bakarman, H.; Al-Admawi, M.; Bech-Hanssen, O.; Di Salvo, G. Pulse-Wave Doppler Interrogation of the Abdominal Aorta: A Window to the Left Heart and Vasculature. *Echocardiography* **2014**, *31*, 543–547. [CrossRef]
12. Klepaczko, A.; Szczypiński, P.; Strzelecki, M.; Stefańczyk, L. Simulation of Phase Contrast Angiography for Renal Arterial Models. *BioMed. Eng. Online* **2018**, *17*, 41. [CrossRef] [PubMed]
13. Polanczyk, A.; Piechota-Polanczyk, A.; Huk, I.; Neumayer, C.; Strzelecki, M. Computational Fluid Dynamics as an Engineering Tool for the Reconstruction of Endovascular Prosthesis Endoleaks. *IEEE Access* **2022**, *10*, 18873–18885. [CrossRef]
14. Polanczyk, A.; Podgorski, M.; Wozniak, T.; Stefanczyk, L.; Strzelecki, M. Computational Fluid Dynamics as an Engineering Tool for the Reconstruction of Hemodynamics after Carotid Artery Stenosis Operation: A Case Study. *Medicina* **2018**, *54*, 42. [CrossRef]
15. Akcimen, M.; Gungor, F.; Beydilli, I.; Soydam Guven, D.; Kesapli, M.; Goksu, E. The Effects of Classic Two-Minute Pressing and Commercial Adhesive Bandages on Ecchymosis Development Following Removal of Intravenous Catheters. *Emerg. Med. Investig.* **2016**, *110*, 4. [CrossRef]
16. Piola, M.; Ruiter, M.; Vismara, R.; Mastrullo, V.; Agrifoglio, M.; Zanobini, M.; Pesce, M.; Soncini, M.; Fiore, G.B. Full Mimicking of Coronary Hemodynamics for Ex-Vivo Stimulation of Human Saphenous Veins. *Ann. Biomed. Eng.* **2017**, *45*, 884–897. [CrossRef]
17. Thomas, A.; Daniel Ou-Yang, H.; Lowe-Krentz, L.; Muzykantov, V.R.; Liu, Y. Biomimetic Channel Modeling Local Vascular Dynamics of Pro-Inflammatory Endothelial Changes. *Biomicrofluidics* **2016**, *10*, 014101. [CrossRef]
18. Winkler, B.; Reineke, D.; Heinisch, P.P.; Schönhoff, F.; Huber, C.; Kadner, A.; Englberger, L.; Carrel, T. Graft Preservation Solutions in Cardiovascular Surgery. *Interact. CardioVasc. Thorac. Surg.* **2016**, *23*, 300–309. [CrossRef]
19. Hicks, C.W.; Obeid, T.; Arhuidese, I.; Qazi, U.; Malas, M.B. Abdominal Aortic Aneurysm Repair in Octogenarians Is Associated with Higher Mortality Compared with Nonoctogenarians. *J. Vasc. Surg.* **2016**, *64*, 956–965.e1. [CrossRef]
20. Janke, D.; Jankowski, J.; Rüth, M.; Buschmann, I.; Lemke, H.-D.; Jacobi, D.; Knaus, P.; Spindler, E.; Zidek, W.; Lehmann, K.; et al. The "Artificial Artery" as In Vitro Perfusion Model. *PLoS ONE* **2013**, *8*, e57227. [CrossRef]
21. Ebrahimi, A.P. Mechanical Properties of Normal and Diseased Cerebrovascular System. *J. Vasc. Interv. Neurol.* **2009**, *2*, 155–162. [PubMed]
22. Polanczyk, A.; Klinger, M.; Nanobachvili, J.; Huk, I.; Neumayer, C. Artificial Circulatory Model for Analysis of Human and Artificial Vessels. *Appl. Sci.* **2018**, *8*, 1017. [CrossRef]
23. Asgharzadeh, H.; Borazjani, I. A Non-Dimensional Parameter for Classification of the Flow in Intracranial Aneurysms. I. Simplified Geometries. *Phys. Fluids* **2019**, *31*, 031904. [CrossRef]

24. Polanczyk, A.; Podgorski, M.; Polanczyk, M.; Piechota-Polanczyk, A.; Stefanczyk, L.; Strzelecki, M. A Novel Vision-Based System for Quantitative Analysis of Abdominal Aortic Aneurysm Deformation. *BioMed. Eng. OnLine* **2019**, *18*, 56. [CrossRef] [PubMed]
25. Polanczyk, A.; Podgorski, M.; Polanczyk, M.; Piechota-Polanczyk, A.; Neumayer, C.; Stefanczyk, L. A Novel Patient-Specific Human Cardiovascular System Phantom (HCSP) for Reconstructions of Pulsatile Blood Hemodynamic Inside Abdominal Aortic Aneurysm. *IEEE Access* **2018**, *6*, 61896–61903. [CrossRef]
26. Iwasaki, K.; Kojima, K.; Kodama, S.; Paz, A.C.; Chambers, M.; Umezu, M.; Vacanti, C.A. Bioengineered Three-Layered Robust and Elastic Artery Using Hemodynamically-Equivalent Pulsatile Bioreactor. *Circulation* **2008**, *118*, S52–S57. [CrossRef]
27. Tong, J.; Holzapfel, G.A. Structure, Mechanics, and Histology of Intraluminal Thrombi in Abdominal Aortic Aneurysms. *Ann. Biomed. Eng.* **2015**, *43*, 1488–1501. [CrossRef]
28. Beenakker, J.-W.M.; Ashcroft, B.A.; Lindeman, J.H.N.; Oosterkamp, T.H. Mechanical Properties of the Extracellular Matrix of the Aorta Studied by Enzymatic Treatments. *Biophys. J.* **2012**, *102*, 1731–1737. [CrossRef]
29. Asgharzadeh, H.; Asadi, H.; Meng, H.; Borazjani, I. A Non-Dimensional Parameter for Classification of the Flow in Intracranial Aneurysms. II. Patient-Specific Geometries. *Phys. Fluids* **2019**, *31*, 031905. [CrossRef] [PubMed]
30. Urbina, J.; Sotelo, J.A.; Springmüller, D.; Montalba, C.; Letelier, K.; Tejos, C.; Irarrázaval, P.; Andia, M.E.; Razavi, R.; Valverde, I.; et al. Realistic Aortic Phantom to Study Hemodynamics Using MRI and Cardiac Catheterization in Normal and Aortic Coarctation Conditions. *J. Magn. Reson. Imaging* **2016**, *44*, 683–697. [CrossRef] [PubMed]
31. Bihari, P.; Shelke, A.; Nwe, T.H.; Mularczyk, M.; Nelson, K.; Schmandra, T.; Knez, P.; Schmitz-Rixen, T. Strain Measurement of Abdominal Aortic Aneurysm with Real-Time 3D Ultrasound Speckle Tracking. *Eur. J. Vasc. Endovasc. Surg.* **2013**, *45*, 315–323. [CrossRef]
32. Piola, M.; Soncini, M.; Prandi, F.; Polvani, G.; Beniamino Fiore, G.; Pesce, M. Tools and Procedures for Ex Vivo Vein Arterialization, Preconditioning and Tissue Engineering: A Step Forward to Translation to Combat the Consequences of Vascular Graft Remodeling. *Recent Pat. Cardiovasc. Drug Discov.* **2012**, *7*, 186–195. [CrossRef]
33. Mundargi, R.; Venkataraman, D.; Kumar, S.; Mogal, V.; Ortiz, R.; Loo, J.; Venkatraman, S.; Steele, T. Novel Sensor-Enabled Ex Vivo Bioreactor: A New Approach towards Physiological Parameters and Porcine Artery Viability. *BioMed Res. Int.* **2015**, *2015*, 958170. [CrossRef]
34. Genovese, K.; Lee, Y.-U.; Lee, A.Y.; Humphrey, J.D. An Improved Panoramic Digital Image Correlation Method for Vascular Strain Analysis and Material Characterization. *J. Mech. Behav. Biomed. Mater.* **2013**, *27*, 132–142. [CrossRef]
35. Gülan, U.; Lüthi, B.; Holzner, M.; Liberzon, A.; Tsinober, A.; Kinzelbach, W. Experimental Investigation of the Influence of the Aortic Stiffness on Hemodynamics in the Ascending Aorta. *IEEE J. Biomed. Health Inform.* **2014**, *18*, 1775–1780. [CrossRef]
36. Kang, J.; Aghilinejad, A.; Pahlevan, N.M. On the Accuracy of Displacement-Based Wave Intensity Analysis: Effect of Vessel Wall Viscoelasticity and Nonlinearity. *PLoS ONE* **2019**, *14*, e0224390. [CrossRef] [PubMed]
37. Pahlevan, N.M.; Tavallali, P.; Rinderknecht, D.G.; Petrasek, D.; Matthews, R.V.; Hou, T.Y.; Gharib, M. Intrinsic Frequency for a Systems Approach to Haemodynamic Waveform Analysis with Clinical Applications. *J. R. Soc. Interface* **2014**, *11*, 20140617. [CrossRef]
38. Li, Y.; Hickson, S.S.; McEniery, C.M.; Wilkinson, I.B.; Khir, A.W. Stiffening and Ventricular–Arterial Interaction in the Ascending Aorta Using MRI: Ageing Effects in Healthy Humans. *J. Hypertens.* **2019**, *37*, 347–355. [CrossRef]
39. Kashyap, V.; Gharleghi, R.; Li, D.D.; McGrath-Cadell, L.; Graham, R.M.; Ellis, C.; Webster, M.; Beier, S. Accuracy of Vascular Tortuosity Measures Using Computational Modelling. *Sci. Rep.* **2022**, *12*, 865. [CrossRef] [PubMed]
40. Pinho, N.; Castro, C.F.; António, C.C.; Bettencourt, N.; Sousa, L.C.; Pinto, S.I.S. Correlation between Geometric Parameters of the Left Coronary Artery and Hemodynamic Descriptors of Atherosclerosis: FSI and Statistical Study. *Med. Biol. Eng. Comput.* **2019**, *57*, 715–729. [CrossRef]
41. Malvè, M.; Gharib, A.M.; Yazdani, S.K.; Finet, G.; Martínez, M.A.; Pettigrew, R.; Ohayon, J. Tortuosity of Coronary Bifurcation as a Potential Local Risk Factor for Atherosclerosis: CFD Steady State Study Based on In Vivo Dynamic CT Measurements. *Ann. Biomed. Eng.* **2015**, *43*, 82–93. [CrossRef]